EXTRACTION OF RECTANGULAR BUILDINGS IN AERIAL IMAGES

Samuel Vinson[1], *Laurent D. Cohen*[2], *and Frédéric Perlant*[1]

[1] EADS Matra Systèmes et Information,
6, rue Dewoitine, 78142 Vélizy-Villacoublay, France
{svinson, fperlant}@matra-ms2i.fr

[2] CEREMADE Université Paris IX Dauphine
Place du Maréchal de Lattre de Tassigny,
75775 Paris cedex 16, France
cohen@ceremade.dauphine.fr

ABSTRACT

This paper introduces an exhaustive process for assisting buildings extraction out of the Digital Elevation Model (DEM) and the orthoimage. We focus on rectangular buildings, which are the most common constructions.

The method is a region-based approach for extracting above-ground structures and for estimating them with rectangles. We establish a relation between the eigenvalues of the covariance matrix and the rectangle dimensions. The Hausdorff measure is used to validate this estimation.

The estimated rectangle shape may be neither well localized nor well sized. We use a parametric model for improving the estimation.

The final rectangle estimation is used to make a precise rendering of the 3D reconstruction of the scene.

Keywords: Building extraction, Rectangular estimation, Deformable Templates, Aerial image

1. INTRODUCTION

In the civil and military fields (infrastructure of telephony, impact studies...), it is increasingly necessary to use realistic models. For examples, authors of [5, 2, 7] have presented automatic methods for terrain modeling (ground, vegetation, and buildings...) based on aerial or satellite photographs. From this modeling and aerial images, the orthoimage, i.e, the vertical view of the scene, is computed (Fig. 1a).

Several works intend to improve building rendering in the Digital Elevation Models (DEM). Brunn et al. [3] minimize a criterion based upon rules of collinearity and right angle. Lin et al. [11] use perceptual grouping to aggregate building edges. Vestri's last work [14] improves accuracy DEM by modifying the method of generation by correlation especially on the building frontages.

Lee et al. [10] present a semi-automatic system to generate 3D models with rectilinear hypotheses. This system attempts to minimize the time and the number of user interactions by defining rules to substract or add rectangles to models.

In our approach, we want to minimize the operator workload. Above-ground structure extraction (vegetation and constructions) (Fig. 1b) is carried out on the DEM by the algorithms presented in [4, 1].

Section 2 deals with estimating the rectangle parameters over any given blob. In section 3, we define a criterion for checking the estimation efficiency. A method which improves the rectangle estimation is introduced in section 4. In the following section, we present an algorithm for splitting complex buildings in several rectangles. At last, we give an overview of this whole process through examples.

2. ESTIMATION OF RECTANGULAR PARAMETERS

We intend to model each above-ground element by a rectangle. The rectangle center of mass and its principal axes are those computed over the element itself. We make an estimate of the two remaining rectangle parameters by means of the element set of points.

The center of mass is given by the first order moment (Eq. 1). The principal axis is computed through the estimation of the second order moments (Eq. 2, Eq. 3).

$$X_g = \frac{1}{K}\sum_i x_i \quad \text{and} \quad Y_g = \frac{1}{K}\sum_i y_i \tag{1}$$

$$M_{xx} = \frac{1}{K}\sum_{i=1}^{K}(x_i - X_g)^2 = \frac{1}{K}\sum_{i=1}^{K} x_i^2 - X_g^2$$
$$M_{xy} = \frac{1}{K}\sum_{i=1}^{K}(x_i - X_g)(y_i - Y_g) = \frac{1}{K}\sum_{i=1}^{K} x_i y_i - X_g Y_g \tag{2}$$

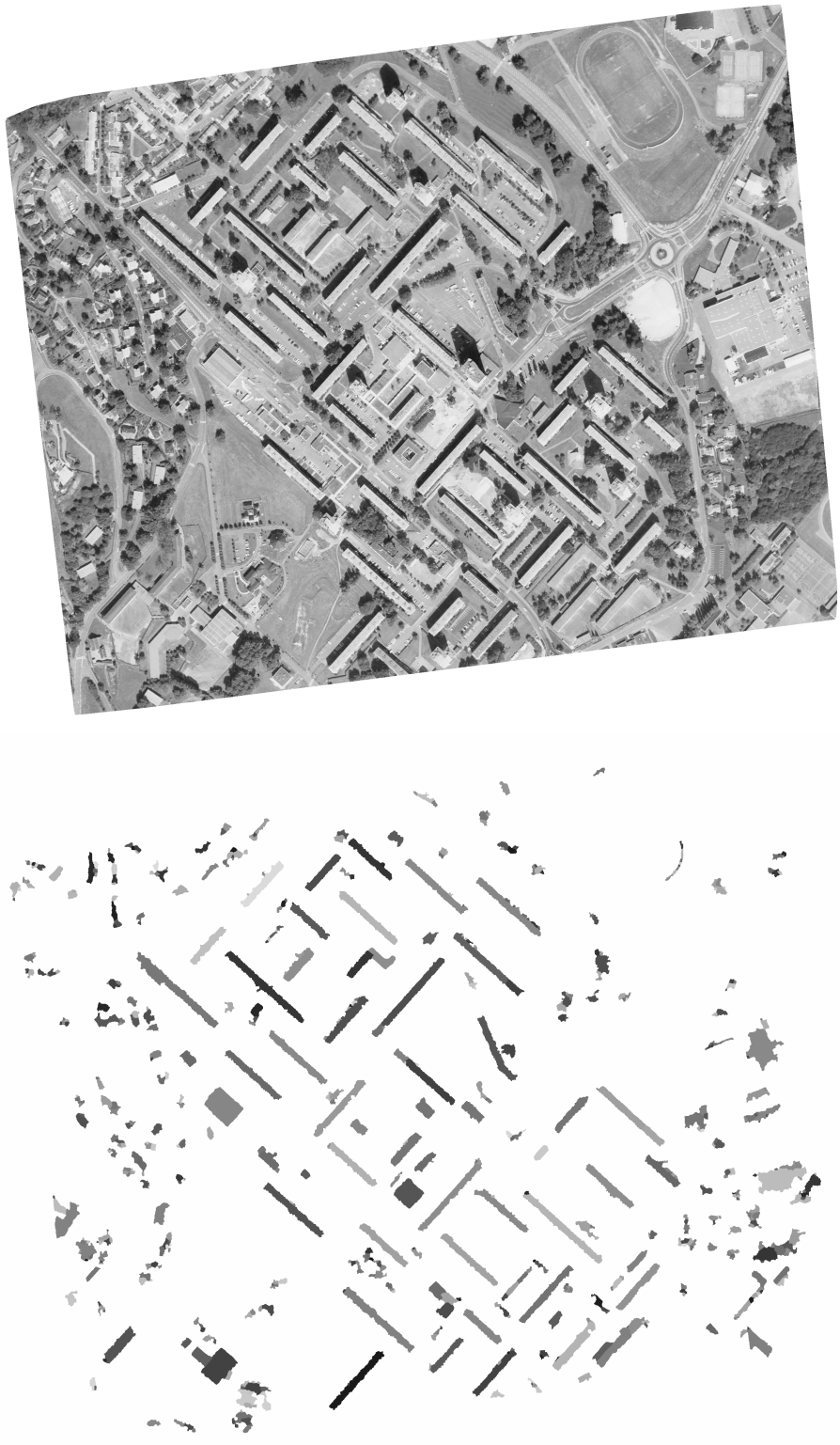

Fig. 1. a. ortho-image b. above-ground

$$\tan 2\theta = \frac{2M_{xy}}{M_{xx} - M_{yy}} \quad (3)$$

The matrix of inertia $\begin{pmatrix} M_{xx} & M_{xy} \\ M_{xy} & M_{yy} \end{pmatrix}$ is made of the second order moments. It is commonly used for estimating the ellipse enclosing the given blob [13]. We intend to apply the matrix properties in order to compute the rectangle sizes. At first, let us consider the matrix diagonalization. It is equivalent to changing the coordinates system. In fact, the diagonalization consists of moving from the Cartesian space to the space orientated towards the blob principal axis.

Let us now consider the eigenvalues. In the case of an horizontal rectangle, the crossed second order moment, i.e. M_{xy}, is nil, and the second order moment M_{xx} (respectively M_{yy}) depends on the blob length (respectively the blob width). There exists a straightforward relationship between the two eigenvalues (Eq. 4) and the length L and the width ℓ (Eq. 5) of rectangle. This result can be extended to any given blob since we know that diagonalization means a change in the coordinate space.

$$\lambda_{max/min} = \frac{M_{xx} + M_{yy} \pm \sqrt{(M_{xx} - M_{yy})^2 + 4M_{xy}^2}}{2} \quad (4)$$

The analytic resolution of Eq. (4) gives the eigenvalues:

$$\lambda_{max} = \frac{L^2 - 1}{12} \quad \text{and} \quad \lambda_{min} = \frac{\ell^2 - 1}{12}$$

Thus,

$$L = \sqrt{12\lambda_{max} + 1} \quad \text{and} \quad l = \sqrt{12\lambda_{min} + 1} \quad (5)$$

The rectangle sizes over the above-ground element are inferred from the eigenvalues. In the case of a square, the principal axis cannot be computed. In fact, $M_{xy} = 0$, so $M_{xx} = M_{yy}$ and θ is always equal to $\frac{\pi}{2}$ (see Eq. 3). However, the orientation of a square shape can be computed by using the Fourier descriptors.

Figure 9 illustrates the method for blobs whose size is over 300 pixels. In the following section, we introduce the criterion we selected for the evaluation of our modeling.

3. MEASURES OF SIMILARITY

Figure 10 shows the superposition of the above-ground blobs and the rectangle estimations. We can see that the modeling is not satisfying when the blob shape is complex. The criterion of similarity that we look for, must act as we do when we visually accept or reject an estimation. Consequently, it must be based on a comparison between sets. We selected the Hausdorff measure among the criteria we studied. The review of criteria, which is not in the scope of this paper, leaded us to a threshold value for validating or rejecting our estimation.

The Hausdorff measure is a comparison between sets. It is equal to the ratio of the intersection area of the two sets $(\mathcal{A}, \mathcal{B})$ to the area of their union (Eq. 6). When two sets are equal, their union also equals to their intersection and the Hausdorff measure is equal to 1. On the contrary, as two sets tend to differ, their intersection decreases whereas their union increases, resulting in a Hausdorff measure decreasing towards 0.

$$M = \frac{\#\mathcal{A} \cap \mathcal{B}}{\#\mathcal{A} \cup \mathcal{B}} \quad (6)$$

where $\#X$ is the number of elements in the set X.

Figure 2 illustrates the Hausdorff measure results for blobs whose size is over 300 pixels. We note that the selection is correct, all blobs that are not rectangular are rejected and only some blobs that could be estimated by a rectangle are excluded.

4. DEFORMABLE TEMPLATES

Previous computations result in a rectangle per above-ground region. When a rectangle is projected onto the orthoimage, its borders do not fully fit the borders of the building. This inaccuracy is the result of the DEM segmentation process as well as the DEM computation itself whose inacurracy is worth a few pixels [4].

Jibrini et al. [9] suggest to improve the borders each one independently of the others. This method requires to limit the border movements in order to keep the borders connected. Fua's work concerning netsnakes with hard-constraints [8] results in 3D structure optimization under constraints of horizontality, of verticality and of right angle. However, the method requires the use of several images, whereas we intend to use one image only, i.e. the orthoimage. The method presented is derived from Yuille et al. work [17] that is a parametric version of Kass et al. snakes [12].

The rectangle parameters, i.e. X_g, Y_g, θ, L and ℓ, define the parametric model (Fig. 3). This model evolves by means of an energy set on the rectangle borders (Eq. 7, 8). This energy is derived from a potential P which is computed over the gradient of the orthoimage. This potential must be minimum at the building edges and greater elsewhere.

$$E = E_{01} + E_{12} + E_{23} + E_{30} \quad (7)$$

$$E_{ij} = \int_0^1 P(X_i + \lambda(X_j - X_i), Y_i + \lambda(Y_j - Y_i))\, d\lambda \quad (8)$$

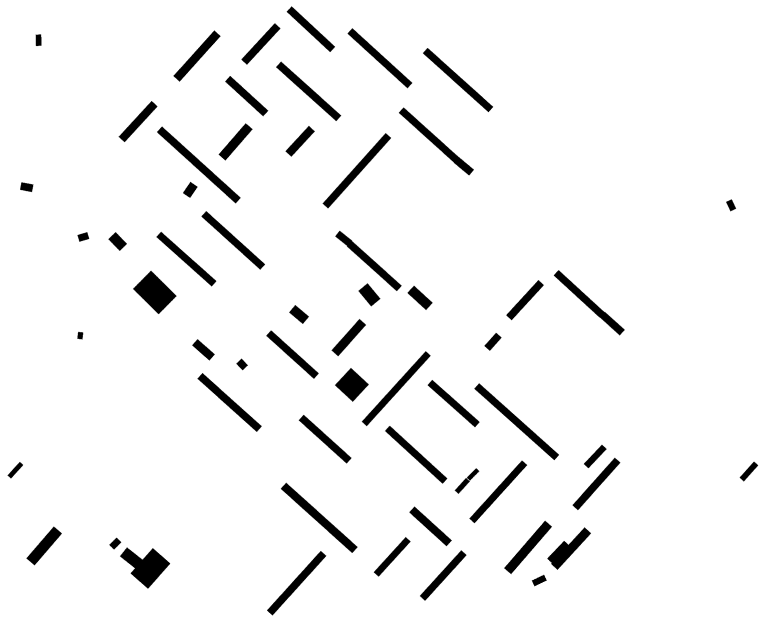

Fig. 2. Rectangle selection

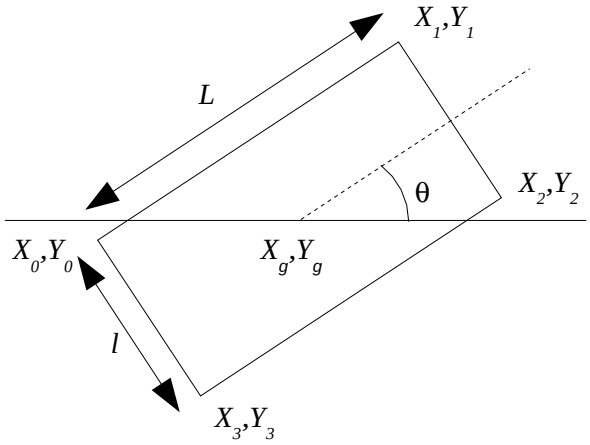

Fig. 3. Five parameters model of a rectangular building

The energy is minimized by means of a gradient descent (Eq. 9). The descent increment is computed at the beginning of the process such that each parameter move is unitary at the first step, i.e. $\alpha \frac{\partial E}{\partial a_k} = \Delta a_k \approx 1$, with $a_k = \{X_g, Y_g, \theta, L, \ell\}$. As per the orientation parameter, the relationship is the following: $\frac{\ell+L}{4}\Delta\theta \approx 1$.

$$\begin{bmatrix} X_g \\ Y_g \\ \theta \\ L \\ \ell \end{bmatrix}^{n+1} = \begin{bmatrix} X_g \\ Y_g \\ \theta \\ L \\ \ell \end{bmatrix}^{n} - \alpha \nabla E \begin{bmatrix} X_g \\ Y_g \\ \theta \\ L \\ \ell \end{bmatrix}^{n} \tag{9}$$

Model evolution requires the computation of the energy gradient. The energy partial derivatives computation is presented in this section for the border P_0P_1. Partial derivatives are computed in the same way for the other borders.

Equation 10 computes the parameters X and Y of the potential P. Coordinates X and Y are function of the five rectangle parameters. Therefore, the partial derivatives of energy E_{01} can be given as a function of these parameters (Eq. 11). These derivatives are a combination of:

- the potential gradients with respect to X and to Y,
- the partial derivatives of X and Y with respect to each parameter (Eq. 11).

$$\begin{aligned} X &= X_0 + \lambda(X_1 - X_0) \\ &= X_g + (-1+2\lambda)L\cos\theta - \ell\sin\theta \\ Y &= Y_0 + \lambda(Y_1 - Y_0) \\ &= Y_g + (-1+2\lambda)L\sin(\theta) + \ell\cos\theta \end{aligned} \tag{10}$$

$$\frac{\partial E_{ij}}{\partial a_k} = \int_0^1 \left(\frac{\partial P(X,Y)}{\partial X} \frac{\partial X}{\partial a_k} + \frac{\partial P(X,Y)}{\partial Y} \frac{\partial Y}{\partial a_k} \right) d\lambda \tag{11}$$

The partial derivatives for the border P_0P_1 are grouped in the Jacobian matrix as the following:

$$f(X_g, Y_g, \theta, L, \ell) = f_{P_0P_1} = \begin{bmatrix} \frac{\partial X}{\partial X_g} & \frac{\partial Y}{\partial X_g} \\ \frac{\partial X}{\partial Y_g} & \frac{\partial Y}{\partial Y_g} \\ \frac{\partial X}{\partial \theta} & \frac{\partial Y}{\partial \theta} \\ \frac{\partial X}{\partial L} & \frac{\partial Y}{\partial L} \\ \frac{\partial X}{\partial \ell} & \frac{\partial Y}{\partial \ell} \end{bmatrix} =$$

$$= \begin{bmatrix} 1 & 0 \\ 0 & 1 \\ -\ell\cos\theta + (1-2\,\lambda)\,L\sin\theta & (-1+2\,\lambda)\,L\cos\theta - \ell\sin\theta \\ (-1+2\,\lambda)\cos\theta & (-1+2\,\lambda)\sin\theta \\ -\sin\theta & \cos\theta \end{bmatrix} \tag{12}$$

Partial derivatives for the three remaining borders can be derived from Eq. 12 by means of a simple rotation of either $\pm\frac{\pi}{2}$ or π. In the case of $\pm\frac{\pi}{2}$ rotations, parameters L and ℓ are exchanged. Equation 13 give the relationship between one border and the function f.

$$\begin{aligned} f_{P_1P_2} &= f(X_g, Y_g, \theta + \frac{\pi}{2}, \ell, L) \\ f_{P_2P_3} &= f(X_g, Y_g, \theta + \pi, L, \ell) \\ f_{P_3P_0} &= f(X_g, Y_g, \theta - \frac{\pi}{2}, \ell, L) \end{aligned} \tag{13}$$

The potential function P is computed over the orthoimage. It must be minimum at the building borders and high elsewhere. Therefore, we compute the reversed gradient norm [6] on the orthoimage. Directional gradients are obtained over the image of potential by applying the Gradient Vector Flow [16]. This method smoothes the potential field in order to set a gradient far away from the borders. Such a method extends the borders power of attraction even if the model is located far away from them.

Figure 4 shows different steps of the process. The top left image presents the rectangular building estimation over the orthoimage. The bottom right image illustrates the deformation process result. We can see, in this example, that the method gives the correct parameters of buildings.

5. COMPLEX BUILDINGS

The buildings may not be rectangular, or may be a composition of rectangles (Fig. 5). We introduce an automatic method which splits a blob into several rectangles. We want to minimize the number of rectangles, the overlap between rectangles and to maximize the size of rectangles. Therefore we split a blob in two regions only, using the orthogonal line of inertia axis which includes the center of mass. Each region is then estimated by a rectangle. A global Hausdorff measure is computed over the rectangles and the blob. The goal is to have the highest global measure, and therefore to optimize the splitting process. Specifically, we proceed by translating the orthogonal line in the direction which increases the region surface of the best rectangular estimation. Again, the global Hausdorff measure is computed over the optimized splitting process. If the measure is not high enough, the splitting is repeated on the badly estimated blobs. Further details on this method are given in [15]. Figure 6 shows that estimation results are improved by using this approach.

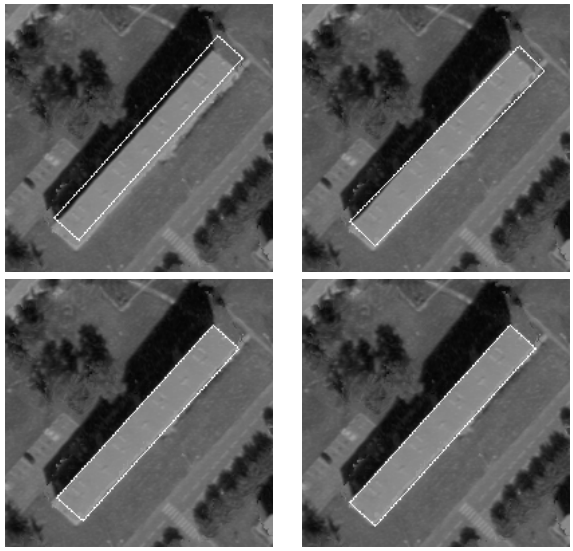

Fig. 4. Evolution process

6. RESULTS

Figure 1a illustrates a vertical view of scene obtain from DEM and several aerial images. Figure 1b shows above-ground. The segmentation process leaves out the vegetation except if they are closed to buildings.

Figure 9 give rectangle estimation for each above-ground element. In figure 10 the rectangle estimation is superposed on above-ground blobs.

Figure 2 illustrates rectangle selection by Hausdorff measure. We note that every bad estimation is rejected.

Figure 6 shows rectangle decomposition result for a complex building.

In figures 7,8 we can see a 3D-reconstruction of the scene with the orthoimage behaving as a texture.

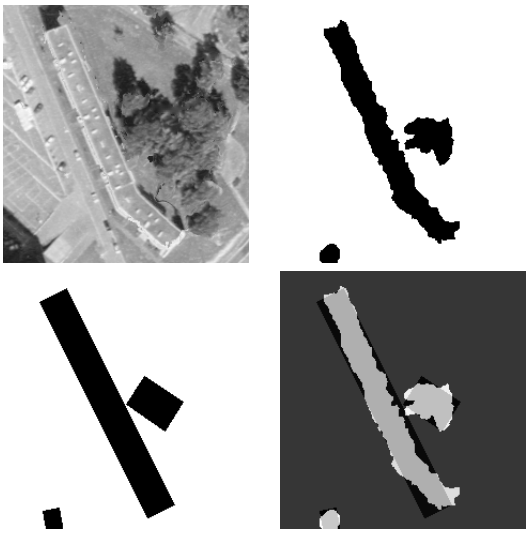

Fig. 5. a. ortho-image b. above-ground c. rectangle estimation c. comparison between rectangle estimation and blob

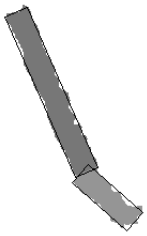

Fig. 6. Rectangle decomposition

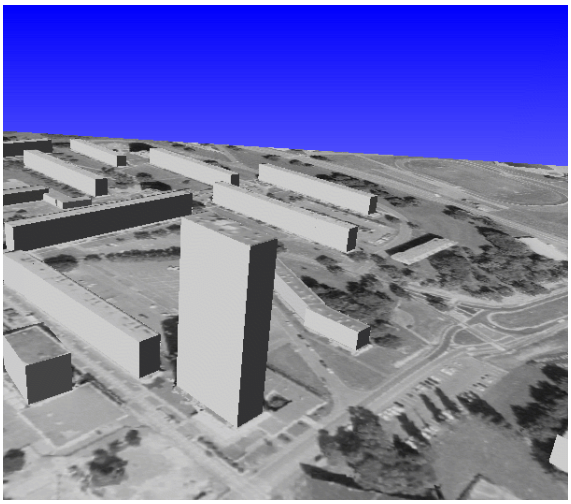

Fig. 7. 3D reconstruction

7. CONCLUSION

This paper describes the processing of the DEM and orthoimage, i.e., the scene vertical view, for the extraction of rectangular buildings as well as buildings which can be decomposed in several rectangles.

The Hausdorff measure saves or rejects our estimation. The design of a rectangular parametric model based upon the orthoimage improves the estimation dimensions and localization.

These automatic processes shorten the operator workload, and compute, to a large extent, the 3D reconstruction of buildings areas.

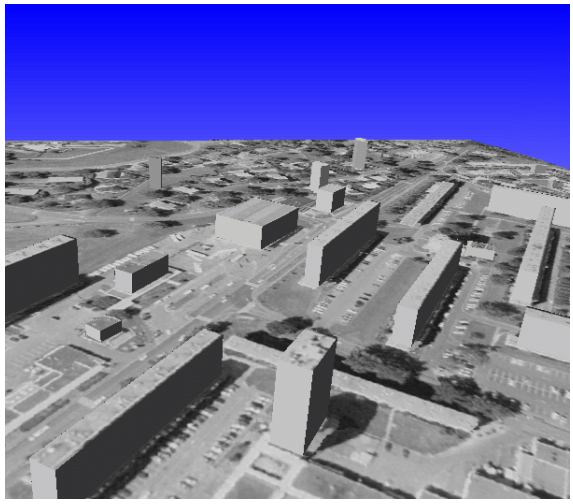

Fig. 8. 3D reconstruction

8. REFERENCES

[1] C. Baillard, O. Dissard, O. Jamet, and H. Maître. Extraction and characterization of above-ground areas in a peri-urban context. In *Proceedings of the IAPR*, pages 159–174, September 1996.

[2] Caroline Baillard and Henri Maître. 3D reconstruction of urban scenes from aerial stereo imagery : A focusing strategy. *Computer Vision and Image Understanding*, 79(3):244–258, december 1999.

[3] Ansgar Brunn, Uwe Weidner, and Wolfgang Förstner. Model-based 2D-shape recovery. In *DAGM Conference on Pattern Recognition*, pages 260–268, 1995.

[4] David Canu. *Vision Stéréoscopique à partir d'un grand nombre d'images : Application à l'imagerie aérienne*. PhD thesis, Université de Rouen, 1997.

[5] David Canu, Jean-Pierre Gambotto, and Jacques A. Sirat. Reconstruction of building from multiple high resolution images. In *Proceedings of International Conference on Image Processing*, September 1996.

[6] Rachid Deriche. Using canny's criteria to derive a recursively implemented optimal edge detector. *The*

Fig. 9. Rectangle estimation

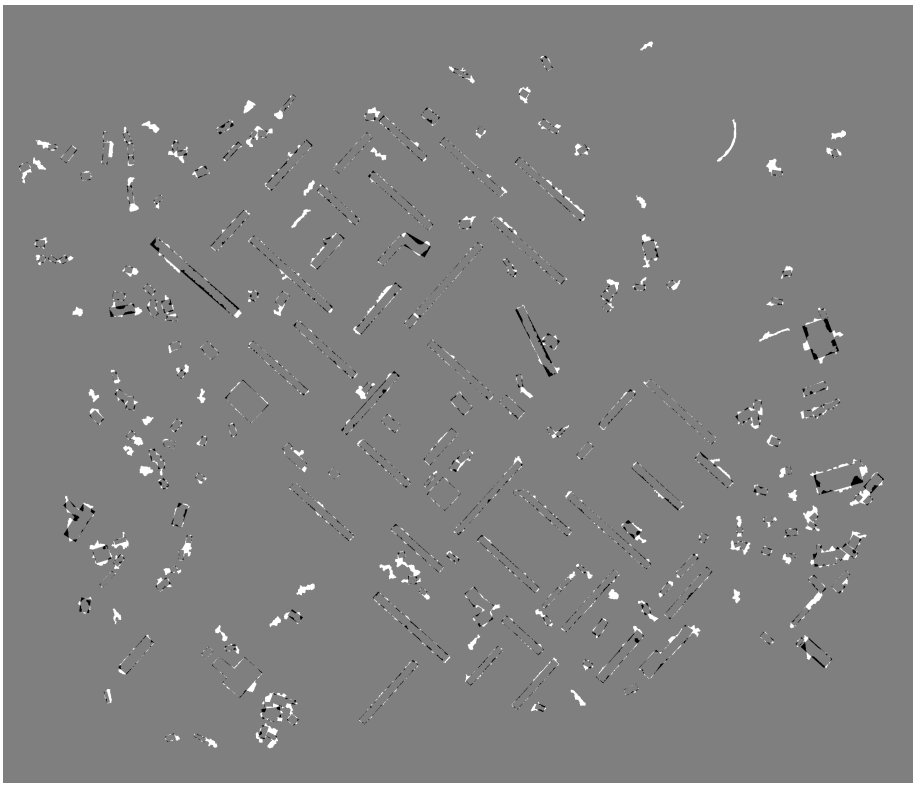

Fig. 10. Difference between rectangle estimation and blobs

International Journal of Computer Vision, 1(2):167–187, 1987.

[7] M. Fradkin, M. Roux, H. Maître, and U.M. Leloglu. Surface reconstruction from multiple aerial images in dense urban areas. In *Proceedings of IEEE Computer Vision and Pattern Recognition*, volume 2, pages 262–267, 1999.

[8] P. Fua and C. Brechbüler. Consistent site modeling; imposing hard constraints on deformable models. Morgan Kaufmann, feb 1996.

[9] Hassan Jibrini, Marc Pierrot-Deseilligny, Nicolas Paparoditis, and Henri Maître. Reconstruction 3D de bâtiments à partir de données 2D cadastrales vectorisées et d'images aériennes. In *Actes de Reconnaissance des Formes et Intelligence Artificielle*, volume 3, pages 299–306, février 2000.

[10] S. C. Lee, A. Huertas, and R. Nevatia. Modeling 3D complex buildings with user assistance. In *WACV*, pages 170–177, 2000.

[11] C. Lin, A. Huertas, and R. Nevatia. Detection of buildings using perceptual grouping and shadows. In *Proceedings of IEEE Computer Vision and Pattern Recognition*, pages 62–69, 1994.

[12] Andrew Witkin Michael Kass and Demetri Terzopoulos. Snakes: Active contour models. In *The International Journal of Computer Vision*, pages 321–331, 1988.

[13] John C. Russ. *The image processing handbook*, chapter 8. CRC Press and Spinger-Verlag, 3 edition, 1999.

[14] Christophe Vestri and Frédéric Devernay. Extraction de façades utilisant la stéréoscopie par corrélation sur des images aériennes transformées. *SFPT*, 153:46–48, Avril 1999.

[15] Samuel Vinson. *Applications des méthodes variationnelles à la reconstruction 3D de sites géographiques*. PhD thesis, Université Paris IX Dauphine, 2001.

[16] Chenyang Xu and Jerry L. Prince. Gradient vector flow : A new external force for snakes. In *Proceedings of IEEE Computer Vision and Pattern Recognition*, pages 66–71, 1997.

[17] Alan L. Yuille, Peter W. Hallinan, and David S. Cohen. Feature extraction from faces using deformable templates. *The International Journal of Computer Vision*, 8(2):99–111, août 1992.